A STUDY OF CHEMICALLY DEPOSITED OXIDE- BASED TERNARY THIN FILM OF ZINC TITANATE ($ZnTiO_3$) DOPED WITH NATURAL DYES AND THEIR POTENTIAL PHOTOVOLTAIC APPLICATIONS.

Calister. N. Eze[abcd*]

[a]Department of Physics, School of Physical Sciences, Federal University of Technology, Minna, Niger State, Nigeria. https://orcid.org/0009-0009-3900-1055.

[b]Department of Industrial Physics, Enugu State University of Science and Technology, Enugu, Nigeria.

[c]Crystal growth laboratory (Nanolab), Department of Physics and Astronomy, University of Nigeria, Nsukka .

[*]Author to whom corresponding should be addressed (C.N. Eze):
E-mail address: marygodchrist@gmail.com

+2348038711901

(This is how to cite this paper: Eze, C.N.)

Abstract:

The ternary metal oxide thin film of $ZnTiO_3$ doped with three different natural dyes were synthesized on glass substrate via solution growth (SG) at room temperature. Chemical baths were used which contained Zinc Sulphate ($ZnSO_4.7H_2O$), Sodium Hydroxide (NaOH), Titanium Chloride ($TiCl_3$), distilled water and calibrated drops per bath of organic dyes: *Lawsonia inermis*, *Beta vulgaries and Jatropha curcas* respectively. Each deposit which was set at a temperature of 80 ^{0}C lasted for 1 h and each deposit was annealed at 400 ^{0}C for 1 h. These deposited nano thin films were characterized for their structural, morphological, optical properties, elemental composition and electronic (chemical) structure and presence of functional groups by means of X-ray diffraction (XRD), Scanning Electron Microscope (SEM), UV-VIS spectrophotometer, Energy Dispersive X-ray Fluoroscopy (EDXRF) and photoluminescence Fourier Transform Infrared Radiation Spectroscopy (FTIR). Polycrystalline thin films were evidenced which marked porosity offered them maximum surface area for dye loading which is critical for photosensitization in dye sensitized solar cells (DSSCs). Such doping presented band gaps of doped $ZnTiO_3$ from 1.84 eV to 3.45 eV depending on dopants applied as against undoped film band gap that was 3.55 eV. The FTIR results showed good photophysical, carboxylate and modification properties of the dyes which helps in sunlight harvesting, anchoring and surface structure modification of the films. The dye influenced the optical properties of the samples and in particular, the reduction of the energy band gap, Eg from an increase in absorption coefficient α, giving high absorbance A, low extinction coefficient k, low reflectance R, which inferred its potential applications in solar energy devices when used in construction, poultry houses, solar cells and DSSCs.

Keywords: Zinc Titanate, Natural Dyes, Chemical Bath Deposition, Potential Applications, Solar Energy Devices.

1. Introduction:

The growth of nanomaterials is being sturdily followed owing to the exceptional characteristics attributed to them like: electronic, magnetic, optical, chemical, and mechanical properties that differ from bulk materials (Dadkhah, Salavati-Niasari, & Mir, 2014) (Sabet & Salavati-Niasari, 2014) (Mir & Salavati-Niasari, 2014) (Mir & Salavati-Niasari, Photovol dye sensitized solar cells: effect of active sites of growth controller on TiO2 nanostructures, 2012).

Generally, materials including ternary metal oxides are doped to increase their solar energy harvesting into electrical energy performance by creating very high surface area for light absorption making the materials to absorb a wider sunlight spectrum and improve its conductivity. When thin films are deposited, they do well in solar energy applications. But they do better when they are doped because the band gap energy (Eg) of the substance is reduced making conduction easy and fast that is, changing band gap to enhance the optical response in the UV to visible light range (Ke, Cheng, Wang, & Wang, 2014) (Xu, et al., (2014) (Patel, 2017) (Suliman, 2007). They are stable and ecologically benign materials used as photocatalyst (Masoud, et al., 2016), in photovoltaics, as photo electrode in dye-sensitized solar cells ($DSSC_S$), to construct metal oxide p-n junction (Faccio, Fernandez-Werner, Pardo, & Mombru, 2011), in antibacterial and photocatalytic activity (Abirami, Kalaiselvi, Kungumadevi, Senthil, & Kang, 2019), in photoprotection activity (Sirajudheen & Gireesh, 2015) and others. Doping is essentially determined by the class of nanomaterial that make up the medium. The doping method will differ in terms of metallic nanoparticles, oxides or semiconductors. But, putting the doping precursor at the start of deposition afore the nucleation of nanoparticles (NPs), is the common style, in the chosen molar ratio and this technique produce nearly 100% result (Eze, Onyia, & Nnabuchi, 2023) (Ezema, 2004).

At the present time, natural dyes are well-thought-out in educational, coloration technology, and industries for the reason that they have the features of being inexpensive, supple, inconsequential, easy removal, easily

synthesized and electronic tunability. It has been studied that Beetroot and many other natural dyes are lightweight and can be used as light-absorbing material in solar cells (Eze, Onyia, & Nnabuchi, 2023) (Kumari, 2020). Natural dyes are chosen more than artificial dyes because they have high absorption coefficient (Eze, Onyia, & Nnabuchi, 2023) (Emre, et al., 2018), have certain chromophore which is a special pigment that help them to attract sunlight energy yet preserve its colour (Paredes-Lopez & DelgadoVargas, 2000). The organic dyes are employed in photovoltaic devices (Paudel, et al., 2018.) (Dhafina & Salleh, 2019) [(Awodugba & Adedokun, 2018.) (Giuseppe, Stefano, Silvia, Oberto, & Caralo, 2009.) (Satoshi, Hideo, Hiroaki, & Shinzaburo, 2009.) (Satoshi, Hiroaki, & Shinzaburo, 2010) (Shuhua, et al., 2017). Doping using dyes changes certain properties of the doped and in the case of ternary oxide materials/thin films, it increases their surface area. Th dye molecules can easily move into the lattices of the thin films of the ternary nanostructures due to its little radial magnitude (Eze, Onyia, & Nnabuchi, 2023). In this work, we have extracted beetroot, henna leaves and leaves of purging nut and used each to dope the ternary ZnTiO3

Due to their tunable features, the several utilizations of $ZnTiO_3$ semiconductor nanostructures include: photocatalysis, gas sensors, energy harvesting and others. Though, the production is faraway more intricate than its binary equivalents, but this is owing to its multicomponent nature (Eze, Onyia, & Nnabuchi, 2023). The intricacy rises even more when targeting cheap and dye-doping procedures via chemical bath deposition methods (Riza & Sepeal, 2019) (Eze, Onyia, & Nnabuchi, 2023)

Many ternary oxides are more stable against acid and natural dyes than their binary oxide counterpart (Eze, Onyia, & Nnabuchi, 2023). They create the very interesting class of materials revealing a diversity of structures and properties. Ternary films often develop good characteristics from the two binary compounds (binary metal compounds) that they consist of (Onyia & Nnabuchi, 2016).

. Scientists lately reported that in the $ZnO–TiO_2$ structure, three compounds occur which are: Zn_2TiO_4 with a cubic spinel crystal arrangement, $ZnTiO_3$ with a hexagonal ilmenite structure ($hZnTiO_3$), and $Zn_2Ti_3O_8$ with a cubic defect spinel structure (Nirmal & Brus, 1999) (Piticescu, Vilarnho, Popescu, & Piticescu, 2006) (Chang, Chang, Chen, & Chen, 2004) (Sirajudheen & Gireesh, 2015).

Nanostructured $ZnTiO_3$ has been deposited via various methods such as sol gel method (Masoud, et al., 2016) (Yang, Akbarzadeh, Maurer, Peterlik, & Schubert, 2012) (Wattanawikkam & and Pecharapa, 2016); conventional solid-state reaction amongst ZnO and TiO_2 with molar ratio 2:1 (Kim, Kim, Valant, & Suvorov, 2001) (Chang, Chang, Chen, & Chen, 2004); co-precipitation method (Sirajudheen & Gireesh, 2015), precipitation method (BUDIGI, NASINA, SHAIK, & AMARAVADI, 2015).

In the above methods employed to deposit ZnTiO3 doped with three different dyes, CBD was not involved hence our reason for the choice of this method. Also, the dyes type was not involved. films formed via CBD process gives superior photovoltaic properties than films deposited by other approaches. These photovoltaic films reveal larger size quantization, reduced crystals, enhanced optical band gap and multipurpose applications. Buffer layers in photovoltaic cells are mainly synthesized via the CBD route following the fact that substrates are not destroyed by CBD process.

2. Related work

M. Salavati-Niasari, et al., worked on Synthesis, characterization, and morphological control of ZnTiO3 nanoparticles through sol-gel processes and its photocatalyst application. They synthesized ZnTiO3 ceramics from the reaction of zinc acetate (Zn (CH3COO)22H2O), tetrabutyl titanate (Ti(OC4H9)4) as precursors also ethanol as the solvent, in the company of benzene-1,3,5-tricarboxylic acid as a different chelating agent by sol-gel method. They examined the consequence of many limitations such as reaction temperature, pH effect, effect of molar ratio of benzene-1,3,5-tricarboxylic acid to tetrabutyl titanate on morphology, size and purity of

products. They characterized the as prepared products by various analyses such as: X-ray diffraction (XRD), scanning and transmittance electron microscopy (SEM, TEM), X-ray energy dispersive spectroscopy (EDS), UV vis and Fourier transform infrared spectroscopy (FT-IR) technique. They studied the photocatalytic degradation using methyl orange (MO) under ultraviolet (UV) light irradiation. They studied application of this product as photocatalyst via degradation of methyl orange (MO) under UV irradiation and percentage of degradation obtained about 70% after 60 min.

C. Yee-Shin, et al., worked on Synthesis, formation and characterization of ZnTiO3 ceramics. They deposited Zinc titanate (ZnTiO3) powders of perovskite structure by conventional solid state reaction by means of metal oxides. They mixed powders of ZnO and TiO2 in a molar ratio of 1:1 in a ball mill and then heated at temperatures from 700 to 1000◦C for various time periods in air. The crystallization temperature of ZnTiO3 powder was ∼820◦C, activation energy for crystallization was ∼327.14kJ/mol and for grain growth was ∼48.84kJ/mol. They observed a transition point when the electrical resistivity was measured versus temperature. Like some ferroelectric materials, a PTCR behavior above the transition temperature was observed with Curie temperature of ∼5◦C.

Chakkaphan Wattanawikkam and Wisanu Pecharapa worked on Sonochemical Synthesis, Characterization, and Photocatalytic Activity of Perovskite ZnTiO3 Nanopowders. They deposited Perovskite zinc titanate (ZnTiO3) nanopowders via the sonochemical method combined with calcinations at 500 °C and 900 °C for 2 h to improve their crystallinity. They studied the effect of calcination temperature on their structural, optical, and photocatalytic properties. The cubic phase and the mixing phase of cubic and hexagonal were observed in sample calcined at 600 °C and 700 °C, respectively, while the spinel ZnTiO3 and rutile TiO2 phase arises in sample calcined over 700 °C. They investigated the valence state by the X-ray absorption near-edge spectroscopy technique, and the corresponding results indicated the existence of Zn2+ and Ti4+ in the powders. They scrutinized The chemical states of the samples by X-ray photoelectron spectroscopy and got average particle size of approximately 20–240 nm. The excellent photocatalytic performance of ZnTiO3 nanoparticle calcined at 700 °C gave complete

degradation Rhodamine B (RhB) in 75 min under ultraviolet light exposure with the k rate of 0.033 min−1 and 55% of decolorization RhB in 210 min under visible irradiation as they discovered. The sample they calcined at 700 °C ensures a good dielectric permittivity with a value 20 and the loss tangent of about 10−2.

3. Experimental Details.

3.1 Material synthesis and dye extraction

In an attempt to obtain $ZnTiO_3$ thin films through chemical deposition method (CBD), Zinc Sulphate and Titanium Chloride were used as precursors. A 0.3M 1.8g of $ZnSO_4.7H_2O$ was measured and dissolved in 55 ml volume of water in a chemical bath under intense stirring to achieve a complete dissolution. 30 ml volume of this solution was put in bath A (b1) for the undoped (AD). A 3 ml volume of $TiCl_3$ added into bath A was vigorously stirred using magnetic stirrer for 10 mins giving a purple colour. Subsequently, 10 ml volume of NaOH from 1.0 M 0.8g of NaOH put into 50 ml volume of water was added into the mixture and stirred for 10 mins. These values are optimized. The same solution was prepared for baths B, C and D for dye-doping. The three different organic dyes [Henna (LL), Beetroot (BR) and purging nut (OO)] were extracted using Sohxlet apparatus for LL and OO where 10ml of ethanol were added to 10 ml of pulverized sample at an extraction temperature of 60 ^{0}C and refluxed for 2hrs and cooling to room temperature giving coloured solutions. Beetroot was grinded gaving a coloured solution. The solutions in baths B, C and D were filtered using filter paper into a container and kept inside a dark cupboard. Three drops of each extracted dye were allowed into beakers B (cca), C (ab) and D (baa) under intensive stirring to dope thin films with dyes. A glass substrate inserted into this mixture for deposition measuring 2.24 x 2.24 x 0.75 was earlier cleansed in concentrated hydrochloric acid, washed in detergent solutions, rinsed in distilled water and left to dry in a dust free environment. The glass slide was pre-heated to 60 ^{0}C, vertically inserted into the solution in A, B, C and D beakers and were suspended from artificial foam which rested on the topmost of the beakers. The mixture containing glass slide was subjected to a temperature of 80 ^{0}C in an oven for 1 h and thereafter annealed at 400 ^{0}C for 1 h.

The crystallinity and diffraction patterns of our product were examined by an advanced X-ray diffractometer (XRD) using the energetic monochromatized $C_uK\alpha l$ radiation source ($\lambda = 1.5406$ Å) in the diffracting range of angle of $10 - 100^0$. It scanned the films as continuously as 2θ varied from$10 - 100^0$ at a step size of 0.02 ^{0} and at a scan step time of 0.2 s. Scanning electron microscope (SEM) was used to study the morphology of the materials. The UV-VIS spectrophotometer was used to study the

optical investigations of the product. The composition of the elements was investigated using Energy Dispersive X-ray Fluoroscopy (EDXRF). The Fourier Transform Infra-Red Spectrometer (FTIR) was used to investigate the chemical/electronic structure and presence of functional group.

Some parameters got from our UV-VIS spectrophotometer highlighted most of the potential applications of this work in solar energy devices hence extinction coefficient, k; reflectance, R; absorbance, A; and energy band gap, Eg were of paramount importance to us. We observed their plots for wavelength range from 229.99 — 1099.78 nm in addition 300 nm to 1100 nm covering part of the UV, all Vis and all NIR regions of the electromagnetic spectrum. They are related thus:

$$\text{Log}_{10}\frac{I}{I_0} = \text{Log}_{10}\left(\frac{1}{T}\right) = A \quad (1)$$

Then $T = 10^{-A}$ (1a)

Also $T = \frac{I}{I_0}$ (1b)

$$R = 1 - A - T \quad (2)$$

$$(\alpha h\nu)^2 = A\,(h\nu - E_g) \quad (3)$$

$$k = \frac{\alpha\lambda}{4\pi} \quad (4)$$

Where, T is transmittance, A is absorbance; λ is wavelength; α is absorption coefficient; Eg is energy band gap; k is extinction coefficient and R is reflectance.

3.2 Characterization

4.0. Results and Discussion

4.1 X-ray diffraction study

This is similar to what was obtained by (Sirajudheen & Gireesh, 2015). Figure 1 illustrates the XRD pattern of the sample deposited via CBD route from the reaction between

Zinc Sulphate ($ZnSO_4.7H_2O$) and Titanium Chloride ($TiCl_3$) solution. The peak positions are consistent with standard diffraction pattern of $ZnTiO_3$ with no secondary crystalline phase observed. The parameters match well with the information for standard JCPDS file card no 00-014-0033 reported by Raveendra *et*

al., 2014. The intense, high, low and narrow peaks observed from the diffraction patterns seen at 2Θ angles of 18.99, 23.84, 32.70, 35.22, 40.40, 48.87, 52.91, 56.75, 61.71, 63.35, 68.65, 70.85, 74.61, 78.54, and 83.93 degrees corresponding to (hkl) orientation of 101, 102, 104, 110, 113, 024, 116, 018, 214, 300, 208, 119, 217, 220, and 314 respectively are characteristic of $ZnTiO_3$. This suggests that incorporation/doping of $ZnTiO_3$ film with dyes doesn't suggest variations in crystalline phase of $ZnTiO_3$ though the peaks appear more intense/enhanced, narrower and higher when compared with the AD. The structural/lattice parameter values seen on table 1.0 shows a crystallite size value, D (nm) of $ZnTiO_3$ calculated to be 47.71815 and was determined from Debye-Scherrer's equation (Bown *et al.*, 2011) thus:

$$D = \frac{K\lambda}{\beta Cos\theta} \quad (6)$$

The Lattice spacing, d (nm) is 2.13366 and was determined from $$d = \frac{\lambda}{2sin\theta} \quad (7)$$

The Dislocation density, δ is 4.39E+14 and was determined from $$\delta = \Delta = \frac{1}{D^2} \quad (8)$$

Also, the Lattice Strain, ε is 2.05254. The interstitial impurities in the material in addition to the non-uniform distribution of d-spaces in the crystallographic plane was observed to be as a result of the existence of lattice strain (Speakman, 2015). It was got from $$\varepsilon = \frac{\beta}{2sin\theta} \quad (9)$$

where, from equations 6 – 9, β is known as the peak's full width at half maximum (FWHM) intensity (ie half the peaks width), K shows a constant identified as the shape factor roughly equivalent to 0.94, λ has a value of (0.1542 nm) or 1.5406 Å and stands for the wavelength of the monochromatic light needed in irradiating the material. D is the crystallite size and Θ is the Bragg's angle.

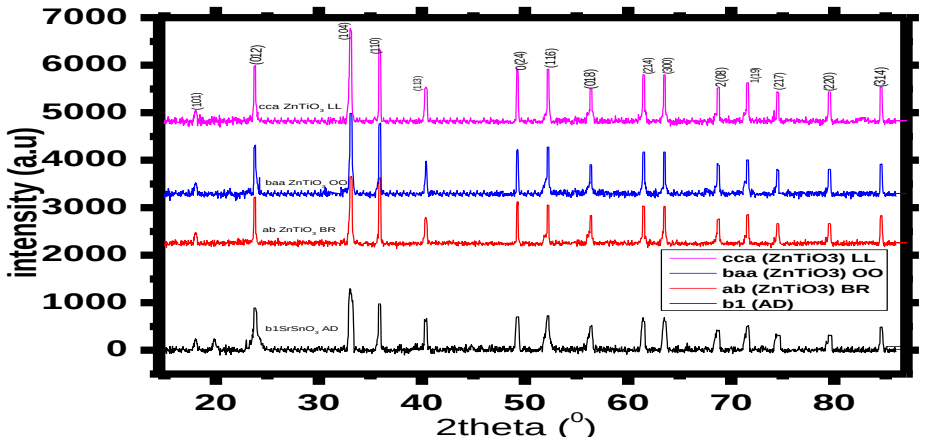

Fig.1: XRD Pattern of CBD $ZnTiO_3$ Thin Films of AD and samples Doped with Different Dyes.

Table 1: The parameters obtained from the XRD Pattern of the $ZnTiO_3$ Thin Films.

Angle 2θ (rad)	θ (rad)	FWHM β	FWHM β (rad)	Crystallite Size, D (nm)	Lattice spacing, d (nm)	Dislocation density, δ	Lattice Strain, ε
14.14423	0.246863	6.26144	0.109283	1.259111	6.256573	6.31E+15	1
36.41831	0.635619	0.4526	0.007899	16.67357	2.465065	3.6E+13	0.343962
30.36886	0.530037	4.78882	0.083581	1.601007	2.940897	3.9E+15	4.411184
33.08979	0.577526	0.34818	0.006077	21.87194	2.705023	2.09E+13	0.293016
46.19613	0.806275	4.91034	0.085702	1.488173	1.963518	4.52E+15	2.878302
49.25005	0.859576	0.26172	0.004568	27.59357	1.84867	1.31E+13	0.142747
52.18181	0.910744	0.35062	0.006119	20.34894	1.751491	2.41E+13	0.178998
56.35713	0.983617	0.30982	0.005407	22.60259	1.631228	1.96E+13	0.144583
47.20715	0.82392	0.01264	0.000221	575.9218	1.923796	3.01E+10	0.007232
228.2804	3.984245	1.66374	0.029038	-1.95282	0.844121	2.62E+15	-0.18641
51.4726	0.898366	6.30332	0.110014	1.135312	1.773945	7.76E+15	3.269031
76.6996	1.338661	6.91527	0.120694	0.900935	1.241496	1.23E+16	2.185155
71.55436	1.248859	0.30972	0.005406	20.80969	1.317575	2.31E+13	0.10745
79.23869	1.382976	13.4018	0.233906	0.456616	1.207965	4.8E+16	4.047215
81.13937	1.416149	1.19219	0.020808	5.061781	1.184398	3.9E+14	0.348111
Average				47.71815	2.133669	4.39E+14	2.05254

4.2 Surface morphology

The SEM micrographs of $ZnTiO_3$ samples AD and samples doped with different dyes are seen in Fig. 2.

The AD (bad/b1) micrograph has non-homogeneous hexagonal structured nanograins with some large sizes sparsely distributed which diminishes with doping with dyes BR (ab) to a more homogenous closely packed pebble-like structure with well-defined boundaries and OO (ba) to a more homogenous spongy-like clustered structure seen in figures 2b and 2c respectively. Film LL (cca) seen in figure 2d, exhibits flakes of spherical nanoparticles, extremely distorted with irregular shapes and with cracks and holes. The dye-doped films reveal porous structures profitable in providing maximum surface area for dye loading and photosensitization suitable in photoanode in DSSCs as against AD with LL being more

porous than others. In this work we have acertained that dyes greatly modify the surface structures of dye-doped samples sugesting increased absorption coefficient, decreased energy band gap, higher absorbance, fairly large crystallite size and low extinction coefficient which results to their potential applications in solar energy devices others (Chang *et al*., 2004; Shalaby, 2011).

M. Salavati-Niasar reveal that the ZnTiO3 700 C, ZnTiO3-800 C and ZnTiO3-900 C have a mean particle size of about 36 nm, 187nm and 500nm, respectively, with spherical like shape.

C. Yee-Shin found the grain size of ZnTiO3 powders calcined at various temperatures was about 0.5–1.0 m.

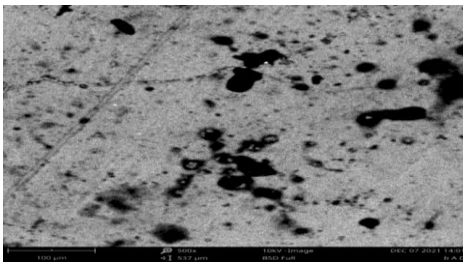

Figure a: As- Deposited film (AD)-bad/b1

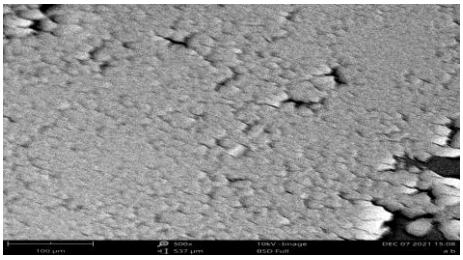

Figure b: Film doped with Dye3 (BR)-ab

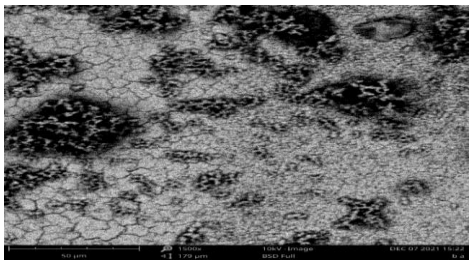

Figure c: Film Doped with Dye2 (OO)-ba

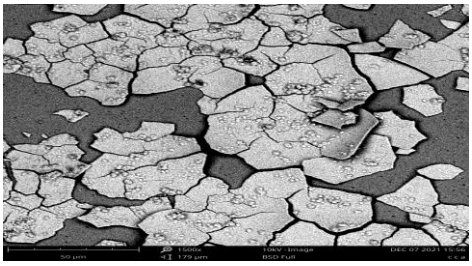

Figure d: Film Doped with Dye1 (LL)-cca

Figure 2. Optical micrographs of $ZnTiO_3$ samples AD, LL, BR and OO.

4.3 Composition study.

The composition of deposited thin films of $ZnTiO_3$ were established by Energy Dispersive X-ray Fluoroscopy (EDXRF) with characteristic spectra of the undoped and doped samples analyzed in figure3. The results show representative elementss like Titanum, Ti; Zinc, Zn and Oxygen, O. and undoped thin films. Other elements like Chlorine, Cl_2; Calcium, Ca; Nickel, Ni; Iron, Fe; etc. are from substrates (glass

slide), dyes, chemicals and handling.

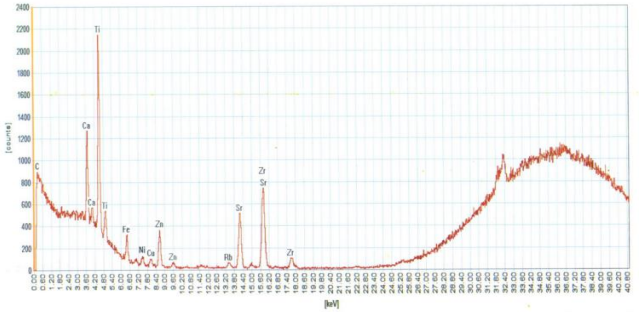

Figure a: As- Deposited film (AD)-bad/b1

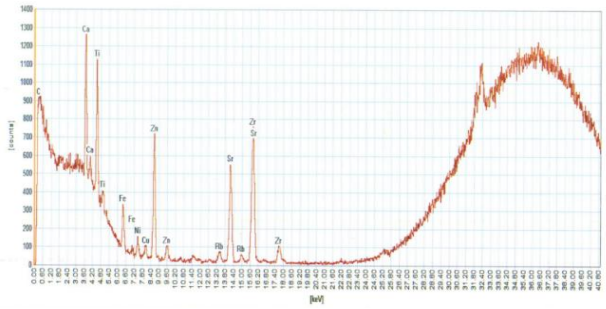

Figure b: Film doped with Dye3 (BR)-ab

Figure 3: The EDXRF Spectrum of Sample ab of $ZnTiO_3$ Nanoparticles Doped with Dye 3 (BR).

4.4 Optical Studies and Band Gap Energy Analysis.

The optical micrographs of films doped with dyes and AD is displayed in figure 4 showing optical results for absorbance, reflectance, energy band gap and extinction coefficient. These parameters are of great importance because they help in identification of their potential application in solar energy devices. The transmittance graph, which is the opposite of reflectance is in line with what was obtained by (Sirajudheen & Gireesh, 2015). It was observed that AD has a lower absorbance than the dye-doped films. The absorption band edges of sample are AD is 398.51 nm, BR is 406.07 nm, OO is 454.06 nm and LL is 602.41 nm found in the visible region. A red shift towards lower energies side was made by the absorption band edges for the dye sensitized samples signifying reduction in the optical band gap of the doped samples. We observed from doped $ZnTiO_3$ that LL has relatively higher absorbance of about 44 %, BR, 39 % and OO, 42 % against AD, 32 %. The variations in the electron-hole in the conduction and valence bands result to a shift of the absorption edge in the UV region (You and Fu, 2016; Agbo *et al.*, 2016; Al-Diabat *et al.*, 2016).

The Eg of both films were determined by looking at the dependence of the absorption coefficient, α on the photon energy, $h\nu$ (Rajashree *et al.*, 2014). Thus equation (3) suffices: $(\alpha h\nu)^2 = A\,(h\nu - E_g)$.

Calculating *hν* and plotting the graph of α against *hν* according to Tauc's model and Davis and Mott model (equation 3) resulted to extrapolation of the linear portion of the plot which gives into the energy axis giving the individual Eg of the materials as AD = 3.55 eV, LL = 3.09 eV, OO = 1.84 eV, and BR = 3.45 eV. The decrease in E_g is an indication that the modification caused by dye could increase the absorption property, strength of the samples and α. Apart from sample OO, the dye-doped samples showed characteristic large band gap of ternary metal oxides used as photoanodes which is advantageous for high efficiency in DSSCs functionality (Lana-Villarreal *et al*., 2007).

The decrease in Eg is due to fairly large crystallite size which does not shift the absorption threshold to longer wavelength since there is no single/separable confinement of electrons and holes. This fairly large crystallite size results in reduced band bending effect. Reduction in Eg is an indication that there is no presence, inside the Eg, of a great density level having energies close to the bands which would have resulted to band trailing as already recommended for many crystalline films. The observed characteristic large Eg of the thin films inferred they have potential applications in solar cell as window layers.

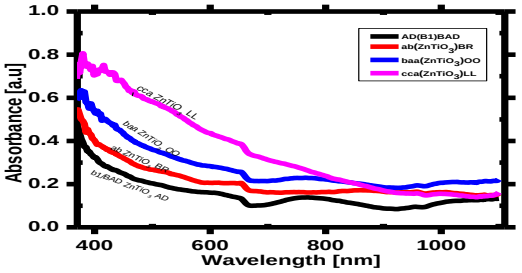

Figure a: Absorbance Graph of films Doped with dyes and AD

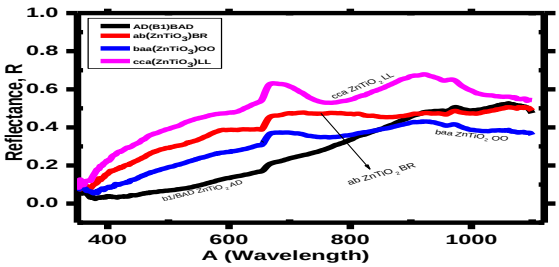

Figure b: Reflectance Graph Films Doped with Dyes and AD

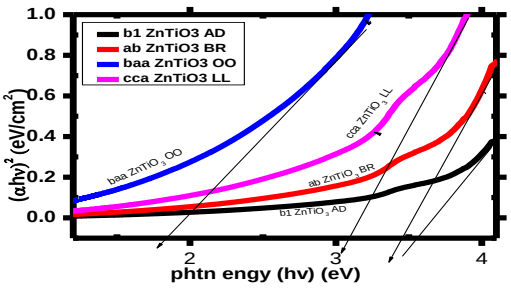

AD (b1) = 3.55 (eV), LL (cca) = 3.09 (eV), OO (baa) = 1.84 (eV) and BR (ab) = 3.45 eV.
Figure c: Energy Band Gap Graph of Films Doped with Dyes and AD

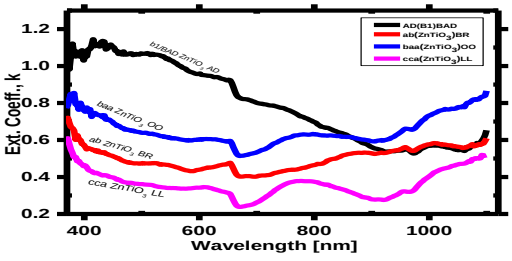

Figure d: Extinction Coefficient Graph of Films Doped with Dyes and AD

Figure 4: The Optical Micrographs of Films Doped with Dyes and AD.

Figure 4d depicts changes of extinction coefficient k of $ZnTiO_3$ samples regarding both AD and doped samples. We observed that k decreases with doping and increase in wavelength. This is attributed to the same reason that absorption coefficient increases with dye doping due to decrease in Eg. The variation of the extinction coefficient k of the sample remains calculated using the equation (4) earlier obtained.

Looking at AD, k decreased from 1.07 to 0.83 as a result of varying the wavelength from 415.8 to 671.5 nm; for BR-ab, k reduces from 0.73 — 0.43 by varying the wavelength from 370.8 to 671.5 nm, for OO-ba, k drops from 0.86 — 0.51 by varying the wavelength from 371.4 — 673.1 nm and for LL-cca, k drops from 0.63 — 0.25 when raising the wavelength from 369.5 — 671.5 nm. The k is lower for dye-doped films than the AD revealing that dyes lower the k of the films as it was seen to improve the crystallinity and reduces the photon disorder/structural imperfections of the films. This reduction in the value of k is as a result of the fundamental absorption of light initiated by the excitation of electrons from the valence band to the conduction band of the doped films. Sample LL has a comparatively lower k and a large energy band gap E_g. This makes it more preferred for application in buffer layer of a Solar Cell or DSSCs than others. However, they all have good qualities to be applied as such. AD has high k, and low η. The behavior observed in figure 3d is typical of most of thin films and is in line with the accounts of some research groups (Vishwakarma and Sahoo, 2017; Kim *et al.*,2017).

4.5 FTIR analysis

The FTIR spectra depicted in figure 4 is the results of the undoped and doped samples. FTIR was used to analyze the Electronic (Chemical) Structure and Presence of Functional Groups of the different dyes used to dope the nanoparticle thin films deposited (Nandiyanto *et al*., 2019; Barry *et al*., 1992). From the outcomes of the results, we inferred that dye LL, OO and BR seen in figures 4a, b and c respectively are

in line with what was reported by other researchers (El-Shishtway, 2009; Narayan, 2012). They presented simple and single bond chemicals with photophysical and carboxylate properties.

Salavati-Niasari, M; in order to study the characteristic vibration bands corresponding to different bonds, the FT-IR spectra was used in the spectral range of 400–4000cm1. It is well known that the characteristic vibration bands corresponding to metal-oxygen bonds be in the range of 400–700 cm1. He found peaks 439cm1 and 537cm1 as the characteristic bands in his findings while we found 3332, 3336 and 3339 as the characteristic bands in our work relating to fig 5a, b, and c of ZnTiO3, corresponding to the stretching vibration of Zn–O and Ti–O bond. Also in his work, the bonds at 3438 and 1633 cm1 were referred to (AOH) groups while in our own case the bonds at 1602.8, 1636.3 and 1640.0 suffices. So, according to appeared peaks, the FT-IR spectrum confirms that ZnTiO3 nanostructures were produced.

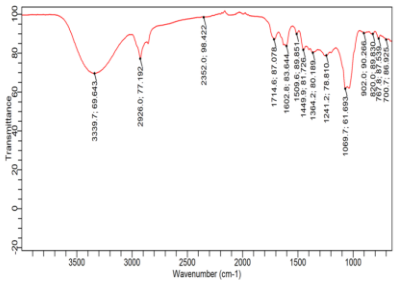

Figure5 a: Mid-IR Transmittance Spectrum Regions of Dye1 Henna (LL)

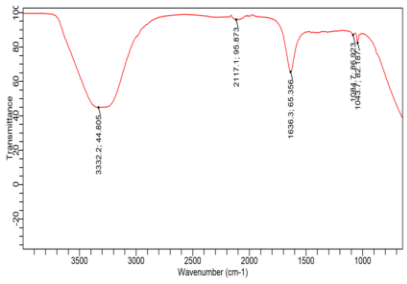

Figure 5b: Mid-IR Transmittance Spectrum Regions of Dye 2 purging nut (OO).

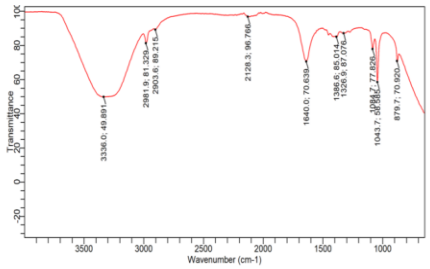

Figure 5c: Mid-IR Transmittance Spectrum Regions of Dye3 Beetroot (BR)

Figure 5: The Mid-IR Transmittance Spectrum Regions of the Dyed Samples and AD.

5.0: Potential Applications of $ZnTiO_3$ in Solar Energy Devices.

The absorbance spectrum revealed higher absorbance emanating from higher absorption band edges of the dye-doped compared with the AD films informing a decreasing energy in the visible region which caused a red-shift. The $ZnTiO_3$ is identified as high absorbance material and can be used in construction

for the roofs in temperate regions where all the UV lights are absorbed and more heat is reradiated and the temperature goes up to reduce Air Conditioner (AC) usages.

The spectral distribution of reflectance showed an average lowered reflectance of 9% for both the AD and dye-doped samples. However, comparatively, dye-doped samples have higher reflectance than the AD which gives high efficiency if used in solar panel by reducing the amount of solar energy that would have reflected. The AD with higher reflectance is used for coating and have greater ability to keep cooler indoor ambient air temperature minus the use of an AC by eradicating solar heat absorption.

All the values have low extinction coefficient, k of the samples but comparatively, the dye-doped have higher k than the AD, thus, the dye-doped materials can be used as window layer for solar cell uses.

All SEM morphologies for doped compared with AD particularly sample LL created pores and cracks/pathways that is beneficial for dye loading and electron transport hence help in photosensitization when used in DSSCs. The dye adsorbed films exhibited better absorption in contrast to its undopped equivalent giving a clue of maximum anchorage of the dyes on the surface of the ternary thin films. However, owing to the crystalline in addition to mesoporous nature as well as anchoring performance, the dye dopped films are seen to be more appropriate as photoanodes for use in DSSCs.

All $ZnTiO_3$ samples have high energy band gap, Eg except sample OO. These high Eg samples can be used in absorption layer of photoelectrode (photoanode) of a DSSCs where these Eg is equal to the Eg of the material(s) (matching of the materials Eg as well as the structure designs for individual film to give the outstanding photochemical output as well as, in this manner, the remarkable conversion efficiency which is a major challenge in fabrication of DSSCs).

The high Eg indicates that the films could equally be utilized in different optoelectronic applications including lasers, light emitting diodes (LED), and in solar cell devices.

5. Conclusion

The thin films of the $ZnTiO_3$ samples doped with diverse natural dyes have been grown on glass substrates via CBD. All the films revealed hexagonal polycrystalline configuration with (104) preferential orientation. The diffraction peak (104) shifts towards greater 2 theta value with doping with dyes. Doping $ZnTiO_3$ with dyes modified the surface morphology greatly. The band gap value decreased from 3.55 eV, for the As- Deposited or non-doped sample, to 3.09 eV, 1.84 eV, and 3.45 eV for LL, OO and BR respectively. These high Eg values , low k, low R, high A and porous surfaces of the films depicts them as candidates for potential applications in solar energy devices.

REFERENCES:

Agbo, P. E., Nwofe, P. A., Ukwu, C. N., Nweke, F. U., (2016). Effect of dye concentration on doped materials. International Journal of Nanomaterials and chemistry, 2: 1.

Agbo, P. E., Nwofe, P. A., Elekwa, C. A., Nnabuchi, M. N., (2016). Effect of dye concentration on doped materials. International Journal of Nanomaterials and chemistry, 2: 1.

Al-Diabat, M. N., Ahmed M. N., Hashim, M. R., Chahrour, M., Bououdina, M., (2016). Dyed samples. Procedia Chemistry, 19: 485.

Augustine, C.N. (2007). Band gap determination of chemically deposited lead sulphide based

heterojunction films. Journal of Non-Oxide Glasses, 9 (3): 85—98.

Augustine, C. and Nnabuchi, M. (2016). The electrical and optical characteristics of Sb-doped and annealed nanocrystalline SnO_2 thin films deposited in CBD techniques. Journal of Ovonic Research, 11 (6): 285—291.

Augustine, C., Chikwenze, R., and Anyaegbunam, F. (2019). Comparative investigation of some selected properties of Mn_3O_4 and CuO/PbS composite thin films. Material Research Express (online), 51: 43—52.

Barry, B.W., Edwards, H.G.M., Williams, A.C. (1992). Fourier transform raman and infrared vibrational study of human skin: Assignment of spectral bands (1992). Journal of Raman Spectroscopy23 (11): 641—645.

Bown, D.F., Pardo, H., Mombru, A.W. (2019). The crystal structures of stannates and titanates thin films deposited using sol-gel method. Journal of Chemical Engineering, 76: 234—241.

Chang, Y.S, Chang Y.H., Chen, I.G., Chen, G.J., Chai, Y.L.,Fang, T.H., Wu, S. (2004). Synthesis, formation and characterization of $ZnTiO_3$. Ceramic International, 30: 2183—2189.

Chen, D., and Ye, J. (2007). $SrSnO_3$ nanostructured synthesis, characterization and photocatalytic properties. Photocatalytic Material Center, National Institute of Materials Science (NIMS), 19: 4585—459.

El-Shishtway, R.M. (2009). Functional dyes and some Hi-tech applications. International Journal of Photoenergy, 1(21):434-441

Energy information administration. (2011). U.S Energy Information Administration. Retrieved march

10, 2021, from international energy statistics: www.eia.go/cfapps/ipdproject/IEDIndex3.cfn.

Ezema, F.I. (2004). Fabrication, optical properties and applications of undoped chemical bath deposited ZnO thin films. Journal of Material Science: Materials in Electronics, 15: 343—350.

Faccio, R., Fernandez-Werner, L., Pardo, H., Mombru, A.W. (2011). Current trends in materials for dye-sensitized solar cells. Recent Patents on Nanotechnology, 5: 46—61.

Kim, D.R., Hwang, D., Son, C.S., Son, Y.G. (2017). The influence of Dye on the energy band gap of materials. Journal of Nanoscience and Nanotechnology, 7: 5016.

Kumarasinghe, P.K.K., Dissanayake, A., Pemasiri, B.M.K., and Dassanayake, B.S. (2017). Effect of post deposition heat treatment on microstructure parameters, optical constants and composition of thermally evaporated CdTe thin films. Mater. Sc. Semicond. Process, 58: 51—62.

Lana-Villarreal, T.E., Boschioo, G., Hagfeldt, A. (2007). Nanostructured zinc stannate as semiconducror working electrodes. J. Phys. Chem., 111: 5549—5556.

Nandiyanto, A.B.D., Oktioni, R., Ragadhita, R. (2019). How to read and interpret FTIR spectroscope of organic material. Indonesia Journal of Science and Technology, 4 (1): 87—118

Narayan, R. (2012). Dye sensitized solar cells based on natural photosensitizers. Renewable and sustainable energy reviews, 16: 208—215.

Nnabuchi, M., and Augustine, C. (2018). Mn_3O_4/PbS thin films: Preparations and effect of annealing. Material Research Express, 5 (3): 0364—0368.

Naoufel, K., and Mounir, K. (2018). Determination and analysis of optical constants and dispersion energy parameters of Zn(S,O) thin films. Materials, Chemistry and Physics, 214: 185—191.

****Nwofe, P.A. (2017). Effect of dye extracts on the optical properties of chemically deposited ZnS thin films. Journal of New Technology and Materials, 07 (02): 93—99.

Onyia, A., and Nnabuchi, M. (2016). Electrical and optical characteristics of Sb-doped and annealed nanocrystalline SnO_2 thin films deposited in CBD technique. Journal of Ovonic Research, 11 (6): 285—291.

Patel, M. (2017). Book of Wind and Solar Power Plant. CRC Press, Reuster.

Puetz, A., Stubhan, R.M., Loesch, O., Hammerberg, E., Wolf, S., Feldmann, C., *et al*., (2011). Organic solar cell incorporating buffer layers from indium doped zinc oxide nanoparticles. Sol. Energy Mater. Sol. Cells, 95: 579—585.

Raveendra, R.S., Osa, D., Nakano, T., Kumara, G.R. (2014). The optical and electrochemical properties of zinc titanate. Journal of Nanotechnology, 45: 456 —465.

Raveendra, R.S., Prashanth, P.A., Bhagya, N.P., Nagabhushana, B.M., Raja Naika, H., Lingaraju, K., Nagabhushana, H., Daruka Prasad, B. (2014). Synthesis, Structural Characterization of Nano $ZnTiO_3$ Ceramic: An Effective Azo dye Adsorbent and Antibacterial Agent. Journal of Asian Ceramic Societies, 2: 357—365.

Riza, M.A., and Sepeal, S. (2019). Synthesis and characterization $SrSnO_3$ using different synthesis methods. Malaysian Journal of Analytical Sciences, 23 (1): 100—108.

Shalaby A., Bachvarova-Nedelcheva, A., Dimitriev, Y., Iordanova., R., Stoyanova, A. (2011). Antibacterial properties of $ZnTiO_3$ prepared by solgel method. Journal of Optoelectronics and Biomedical Materials, 3(2): 39 —44.

Speakman, V.N. (2015). A general study of imperfections in thin films: the titanates. Chalcogen Letters, 98: 875—882.

Suliman, A.E. (2007). Preparation of ZnO nanoparticle and nanosheets and their application to dye sensitized solar cells. Sol. Energy Mater Sol. Cells, 91 (18): 1658—1662.

Vishwakarma, R., and Sahoo, A. (2017). Effect of dyes on the energy band gap and application of materials. Journal of Advanced Physics, 6: 274.

Wei, L.Y. (2015). Effect of different donor groups in bis (6-methoxylpyridin-2-yl) substituted co-sensitizer on the performance of N719 sensitized solar cells. RSC Advances, 5 (117): 96934—96944.

You, R. W. and Fu, Y. P. (2016). Doping. Adv., Tech., Innovation, 2: 95.